

**Vibrational memory in quantum localized states**Y. Ajili,<sup>1</sup> T. Trabelsi,<sup>1</sup> O. Denis-Alpizar,<sup>2</sup> T. Stoecklin,<sup>2</sup> A. G. Császár,<sup>3</sup> M. Mogren Al-Mogren,<sup>4</sup>  
J. S. Francisco,<sup>5,\*</sup> and M. Hochlaf<sup>1,†</sup><sup>1</sup>*Université Paris-Est, Laboratoire Modélisation et Simulation Multi Echelle, MSME UMR 8208 CNRS,  
5 boulevard Descartes, 77454 Marne-la-Vallée, France*<sup>2</sup>*Institut des Sciences Moléculaires, Université de Bordeaux, CNRS UMR 5255, 33405 Talence Cedex, France*<sup>3</sup>*MTA-ELTE Complex Chemical Systems Research Group, H-1117 Budapest, Pázmány Péter sétány 1/A, Hungary*<sup>4</sup>*Chemistry Department, Faculty of Science, King Saud University, P.O. Box 2455, Riyadh 11451, Kingdom of Saudi Arabia*<sup>5</sup>*Department of Chemistry and Department of Earth and Atmospheric Sciences, Purdue University, West Lafayette, Indiana 47906, USA*  
(Received 2 March 2016; published 24 May 2016)

The rovibrational eigenenergy set of molecular systems is a key feature needed to understand and model elementary chemical reactions. A unique class of molecular systems, represented by an  ${}^4A'$  excited electronic state of the  $[H,S,N]^-$  system comprising several distinct dipole-bound isomers, is found to contain both bent and linear minima separated by relatively small barriers. Full-dimensional nuclear-motion computations performed in Jacobi coordinates using three-dimensional potential energy surfaces describing the stable isomers and the related transition states yield rovibrational eigenstates located both below and above the barriers. The rovibrational wave functions are well localized, regardless of whether the state's energy is below or above the barriers. We also show that the states preserve the memory of the isomeric forms they "originate from," which is signature of a strong vibrational memory effect above isomerization barriers.

DOI: [10.1103/PhysRevA.93.052514](https://doi.org/10.1103/PhysRevA.93.052514)**I. INTRODUCTION**

A foundational concept of chemistry is that many chemical events involving nuclei occur on potential energy (hyper) surfaces (PESs), which arise only within the Born-Oppenheimer separation of nuclear and electronic motions. A corollary to this doctrine is that simple PESs—those with few stationary points (minima and transition states)—lead, at least at low excitation, to simple nuclear dynamics, whereas complex PESs—those with a considerable number of stationary points—lead to intricate dynamic behavior, particularly for potentials with several wells. If two equivalent wells are separated by a relatively small barrier, tunneling splitting of the rovibrational energy levels can be observed, such as for the ground electronic state of ammonia,  $NH_3$  [1]. A nonsymmetric double-well potential characterizes the ground electronic state of the  $[H,C,N]$  system and the  $HCN \leftrightarrow HNC$  unimolecular isomerization reaction [2–4]. When the system has sufficient energy for the two wells to "interact," the states above the barrier may belong to one or the other well or exist as a mixture of the two. In 1987, Bacic *et al.* [5] investigated the  $HCN/HNC$  system in a one-dimensional pseudopotential where localized rovibrational wave functions were noticed below and above the  $HCN \leftrightarrow HNC$  isomerization barrier. Another interesting case is that of the  $[H,H,C,O]$  system, which has two dynamically important nonsymmetric wells: formaldehyde,  $H_2CO$ , which corresponds to the global minimum, and *trans*-hydroxycarbene,  $HCOH$ , which can tunnel through a barrier larger than  $100 \text{ kJ mol}^{-1}$ , simplifying the expected high-energy dynamics considerably [6]. The acetylene  $\leftrightarrow$  vinylidene isomerization constitutes another interesting example [4]. Herman and Perry [3] studied acetylene isomerization and

showed recently the creation of new vibrational modes and intramolecular vibrational-rotational energy redistribution over multiple time scales when considering levels below and above the isomerization barrier. Prior to that, Bowman and co-workers [7] studied this process in a reduced dimensionality potential that is minimized with respect to other degrees of freedom, such that the resulting potential contains both the acetylene and vinylidene minima. Localized vibrational levels above the isomerization barrier were predicted. Another relevant study is the combined theoretical and experimental investigation of Continetti and co-workers [8] into the dissociation dynamics of the tetra-atomic  $FH_2O$  system. They provided snapshots of the  $F + H_2O \rightarrow HF + OH$  reaction from wells to barriers. Recent developments in the dynamic study of molecular collisions allow the nature and behavior of molecular systems above the dissociation limits to be fully characterized, which has improved our understanding of the fundamental processes occurring during molecular collisions. In these studies, the agreement between the experimental and first-principles results is striking (see, e.g., Refs. [9–12]).

Occasionally even simple, one-dimensional (1D) physical models may lead to surprisingly complex dynamic behavior. Aleiner *et al.* [13] recently provided an example of unexpected localization in the case of a 1D gas of short-range interacting bosons in the presence of disorder. Their work showed that a 1D gas can theoretically undergo a finite-temperature phase transition between two distinct states: fluid and insulator. In the insulating state, bosons are distributed among "lakes" located exponentially far from one another without the possibility of hopping between the lakes. These lakes may be connected to the lobes of the rovibrational wave functions, where the nuclei are constrained to move, even above the barriers. Another example for localized bound and unbound states is the case of GaAs wells [14] observed after injecting quasimonoenergetic ballistic electrons into GaAs potential wells of various thicknesses. These experiments showed that

\*francisc@purdue.edu

†hochlaf@univ-mlv.fr

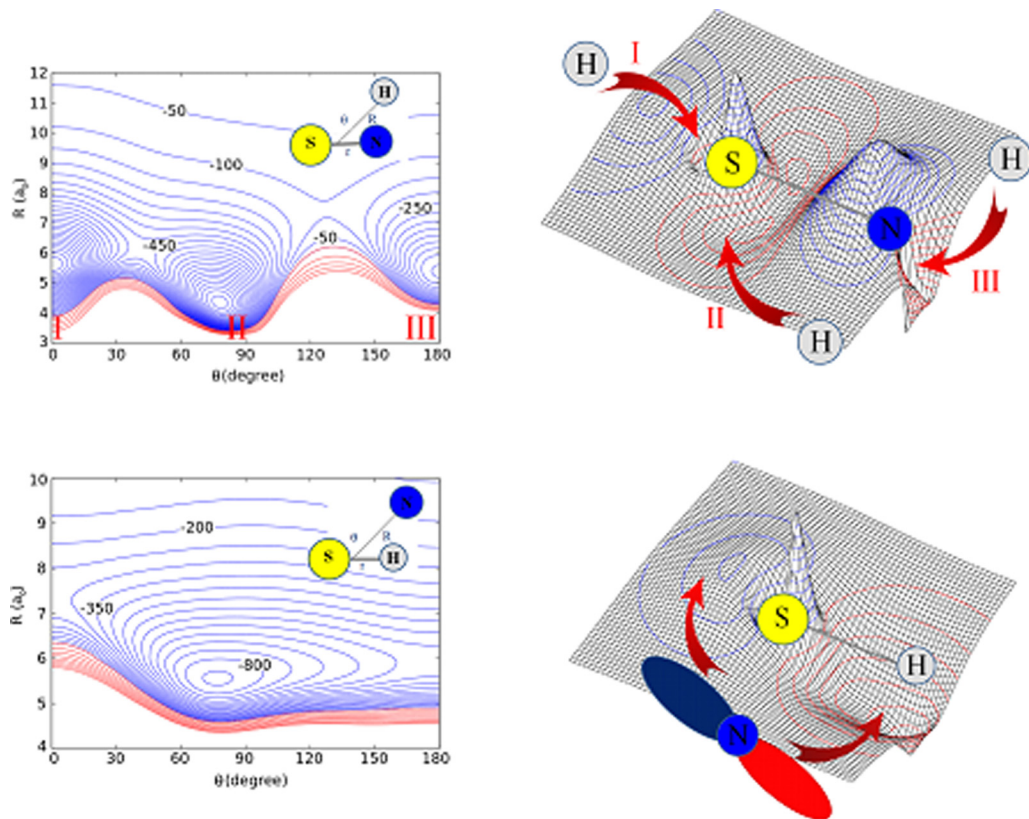


FIG. 1. Top left: (R)CCSD(T)-F12/aug-cc-pVTZ contour plots of the PES of the  $\text{SN}\cdots\text{H}^-$  quartet electronic state along the Jacobi coordinates  $R$  (in units of  $a_0$ , where  $1a_0 = 1 \text{ bohrs} = 0.5292 \text{ \AA}$ ) and  $\theta$  (in units of degrees), where  $r(\text{SN})$  is fixed at 2.96 bohrs. The step between the contours is  $50 \text{ cm}^{-1}$ . The zero energy corresponds to the energy of the  $\text{SN}^-(X^3\Sigma^-) + \text{H}(^2S)$  asymptote. Top right: LUMO of  $\text{SN}^-$  interacting with the  $1s$  atomic orbital of hydrogen. Bottom left: (R)CCSD(T)-F12/aug-cc-pVTZ contour plot of the PES of the  $\text{SH}\cdots\text{N}^-$  ( $^4A''$ ) electronic state along the Jacobi coordinates  $R$  (in units of  $a_0$ ) and  $\theta$  (in units of degrees), where  $r(\text{SH})$  is fixed at 2.53 bohrs. Right: HOMO of  $\text{SH}^-$  interacting with the  $2p$  atomic orbital of N. The step between the contours is  $50 \text{ cm}^{-1}$ . The zero energy corresponds to the energy of the  $\text{SH}^-(X^1\Sigma^+) + \text{N}(^4S)$  asymptote. The red arrows indicate the favorable interactions between the frontier orbitals of  $\text{SH}^-/\text{SN}^-$  and  $\text{N}/\text{H}$ .

the corresponding spectra are structured for bound states, as expected, and for the relatively large number of unbound states located in the virtual region where peaks indicate their localization [14]. Spectral localizations were also observed in solid-state quantum dots by Chen *et al.* [15]. In the literature, there were several attempts using 1D potential models [2,5,14–16] to answer the fundamental question of whether simple localized states exist above barriers and specifically whether the localization of vibrational states could occur systematically in chemical systems above a barrier.

To go beyond these previous 1D and reduced dimensionality treatments, we perform full three-dimensional (3D) potential through the investigation of the 3D PESs of the  $^4A''$  of the long-lived, weakly bound  $\text{SN}\cdots\text{H}^-$  and  $\text{SH}\cdots\text{N}^-$  isomeric complexes, which can be formed after cold collisions between  $\text{SN}^-$  and H or  $\text{SH}^- + \text{N}$  [17]. These 3D PESs are first mapped and then incorporated into nuclear-motion computations. Subsequently, we present a detailed analysis of the nature of the eigenstates and energies, irrespective of whether the state's energy is below or above the potential barriers. Our analysis shows that the rovibrational wave functions are localized in character, not only below but also above the isomerization barriers and exhibit strong memory effects of the molecular minimum-energy structures.

## II. METHODOLOGIES

### A. Potential energy surface (PES) generation

The procedure established by Hochlaf and co-workers [18–23] for the deduction of accurate multidimensional interaction potentials in van der Waals systems with low computational cost is used. Specifically, the electronic computations are performed using the explicitly correlated coupled cluster method with single, double, and perturbative triple excitations [CCSD(T)-F12] (approximation b) [24,25], as implemented in MOLPRO [26]. In these computations, the atom-centered, fixed-exponent, augmented correlation-consistent aug-cc-pVTZ Gaussian basis set [27,28] is employed in connection with the corresponding auxiliary basis sets and density fitting functions [29,30], which correspond to the default basis sets of Peterson and co-workers, CABS(OptRI) (cf. Ref. [17] for more details). For both molecular species, the 3D PESs are calculated for  $\theta$  angles ranging from  $0^\circ$  to  $180^\circ$  with a uniform step of  $10^\circ$ . For  $\text{SH}\cdots\text{N}^-$ ,  $R$  is varied from 3.7 to 40 bohrs, and the  $r(\text{SH})$  distance is varied from 2.51 to 3.11 bohrs. For  $\text{SN}\cdots\text{H}^-$ ,  $R$  is varied from 3.1 to 40 bohrs, and  $r(\text{SN})$  is between 2.7 and 3.2 bohrs. In total, 3589 (2593) *ab initio* energies are computed for nonequivalent geometries of  $\text{SH}\cdots\text{N}^-$  ( $\text{SN}\cdots\text{H}^-$ ). The basis set superposition error

(BSSE) is corrected at all geometries using the Boys and Bernardi [31] counterpoise scheme.

### B. Analytical representation and description of the PESs

The analytical models of the 3D PESs are obtained using a fitting procedure based on the reproducing kernel Hilbert space (RKHS) approach [32]. The interaction energies are expressed as

$$V(R, r, \theta) = \sum_{i=1}^{N_R} \sum_{j=1}^{N_r} \sum_{k=1}^{N_\theta} b_{ijk} q^{2,3}(R_i, R) q^{2,3}(r_j, r) q_1(z_k, z), \quad (1)$$

where  $z = 0.5(1 - \cos \theta)$ ,  $b_{ijk}$  are linear coefficients and  $N_R = 41$ ,  $N_r = 7$ , and  $N_\theta = 12$  denote the number of *ab initio* data points calculated along the  $R$ ,  $r$ , and  $\theta$  Jacobi coordinates. The expressions of the 1D reproducing kernel functions  $q^{2,3}(R_i, R)$ , which vary asymptotically in  $1/R^4$  for large values of  $R$  and of  $q_1(z_k, z)$ , are given in [33].

### C. Calculations of the rovibrational eigenstates and wave functions

Two independent methods are used to solve the nuclear-motion problem: (i) close coupling and (ii) variational computations. The close-coupling method is incorporated in BOUND [34], which was used to obtain a first set of rigid rotor-bound states energies. This method relies on the fact that the coupled equations needed for scattering calculations are identical to those for bound states, only differing in the applied boundary conditions. In these computations, the rotational constants of the SN and SH molecules were set to  $B_0 = 0.7696 \text{ cm}^{-1}$  and  $B_0 = 9.325 \text{ cm}^{-1}$  [35], respectively. A  $0.1 \text{ cm}^{-1}$  convergence of the first 100 bound-state energies was achieved using 44 and 20 rotational basis functions for the  $\text{SN} \cdots \text{H}^-$  and  $\text{SH} \cdots \text{N}^-$  complexes, respectively. The difference in the size of the rotational basis set required to reach convergence exists because the angular variation of the PES is more anisotropic for  $\text{SN} \cdots \text{H}^-$  than for  $\text{SH} \cdots \text{N}^-$ . To verify these results and obtain the associated wave functions, we independently perform variational 3D calculations as detailed in previous studies (see, for example, [18]). The angular part of the wave function is taken to be the usual  $|j l J M\rangle$  coupled basis set in Jacobi coordinates in the space-fixed frame, where  $j$ ,  $l$ , and  $J$  are the quantum numbers associated with the rotation of the diatom, the relative, and the total angular momentum of the complex, respectively.  $M$  is the projection of  $J$  along the space-fixed  $z$  axis. For the radial part, we use a Chebychev [36] DVR representation of both the intermolecular  $R$  and diatomic  $r$  Jacobi coordinates. The DVR grid along  $R$  includes 600 points between 3.1 and 30 bohrs for  $\text{SH} \cdots \text{N}^-$  and 900 points between 3.2 and 22 bohrs for  $\text{SN} \cdots \text{H}^-$ . A Gauss Hermite quadrature of ten points is used to calculate the diatomic vibrational part of the intermolecular potential matrix elements. The sizes of the rotational basis sets used for these variational calculations are the same as those of the close-coupling calculations. Good agreement between the two calculations is obtained, and the spacing between the bound states is confirmed.

TABLE I. Calculated rovibrational energy [ $E(\text{cm}^{-1})$ ] levels of  $\text{SN} \cdots \text{H}^- (^4A'')$  for  $J = 0$  and 1, together with their tentative assignment. Isomer I is for the linear  $\text{H} \cdots \text{SN}^-$  complex. Isomer II is for the bent complex. Isomer III is for the  $\text{SN} \cdots \text{H}^-$  linear complex.  $\nu_s$  corresponds to van der Waals vibrational stretching, and  $\nu_b$  is for van der Waals vibrational bending. These energies are given with respect to the  $\text{SN}^- (X^3\Sigma^-) + \text{H} (^2S)$  asymptote energy. Levels in black exhibit a bent molecule pattern, regardless of whether they are below or above the potential barriers. Levels in red (stretching) and blue (bending) correspond to a linear-type molecule, regardless of whether they are below or above the potential barriers. In the SM [38], we provide the full set of computed levels up to dissociation. \* denotes an anharmonic resonance.

Isomer	Assignment ( $\nu_s, \nu_b$ )	$J = 0$		$J = 1$	
		E	Parity ( $\epsilon$ )	E	Parity ( $\epsilon$ )
I	(0,0)	-832.33	+	-830.75	-
				-789.48	-
II	(0,0)	-789.93	+	-787.08	-
				-786.01	+
I	(0,1)			-630.83	+
				-630.64	-
				-550.00	-
II	(0,1)	-549.95	+	-547.71	-
				-546.15	+
I	(1,0)	-540.64	+	-539.02	-
				-481.27	-
II	(1,0)*	-480.66	+	-479.30	-
				-477.17	+
I	(0,2)*	-468.33	+	-467.28	-
				-387.90	+
I	(1,1)*			-387.76	-
III	(0,0)	-376.43	+	-374.81	-
				-369.90	-
II	(0,2)	-369.99	+	-366.90	-
				-365.55	+
				-333.23	-
I	*			-332.90	+
I	(2,0)*	-321.62	+	-320.09	-
I	*	-300.46	+	-299.86	-

The synthetic microwave–far infrared ( $\mu\text{w}$ -far IR) spectra of  $\text{SN} \cdots \text{H}^-$  and of  $\text{SH} \cdots \text{N}^-$  are generated using the recently developed approach, as described in Ref. [37].

## III. RESULTS

### A. Nature of the 3D PESs of the $\text{SN} \cdots \text{H}^-$ and $\text{SH} \cdots \text{N}^-$ anions

The 3D PESs of the lowest quartet electronic states of the  $\text{SH} \cdots \text{N}^-$  and  $\text{SN} \cdots \text{H}^-$  anions are generated in Jacobi coordinates  $r$ ,  $R$ , and  $\theta$  (see Fig. 1), using the state-of-the-art (R)CCSD(T)-F12/aug-cc-pVTZ level of electronic structure theory, from which analytical representations of these 3D PESs are deduced. These surfaces are then used within two independent nuclear-motion codes to compute the energies and

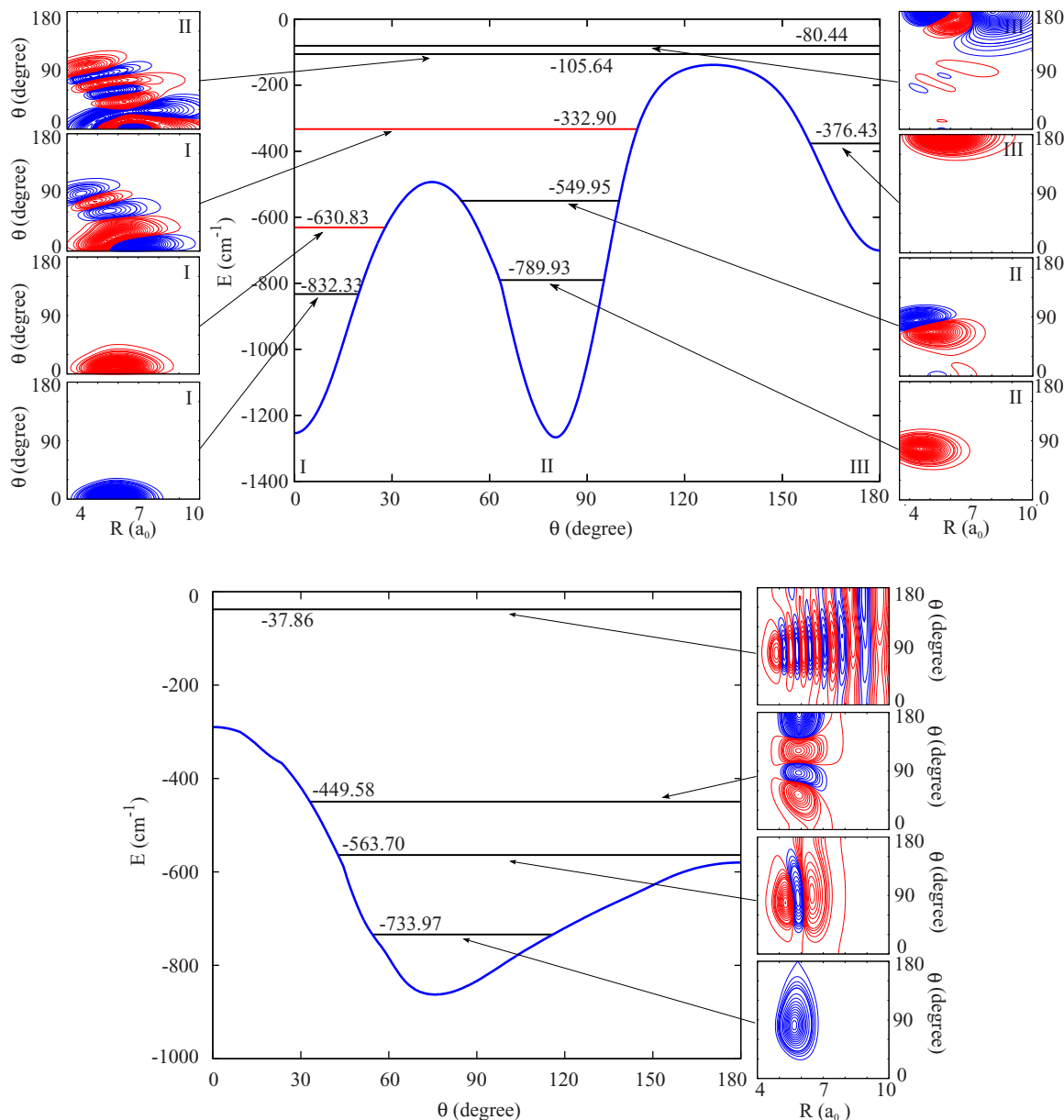


FIG. 2. Selected rovibrational wave functions from the SM [38] for  $\text{SN} \cdots \text{H}^-$  (top) and  $\text{SH} \cdots \text{N}^-$  (bottom) complexes and their localization in the corresponding potential (blue curve), where  $r$  is relaxed. The horizontal black lines indicate the levels appearing when  $J \geq 0$ , whereas the red horizontal lines represent those appearing only when  $J \geq 1$ .  $R$  is in units of  $a_0$  and  $\theta$  is in units of degrees.  $E$  is the energy in units of  $\text{cm}^{-1}$ .

wave functions for both anionic systems [18,34]. The results independently confirm the observed features.

The 3D PESs of  $\text{SN} \cdots \text{N}^- (^4A'')$  and of  $\text{SH} \cdots \text{N}^- (^4A'')$  (Fig. 1) are both strongly anisotropic. The less-structured PES belongs to  $\text{SH} \cdots \text{N}^- (^4A'')$  and includes one potential well with a bent arrangement ( $r_e = 2.71$  bohrs,  $R_e = 5.60$  bohrs, and  $\theta_e = 78.0^\circ$ ) (1 bohr =  $1a_0 = 0.5292 \text{ \AA}$ ). The pure electronic dissociation energy is  $D_e = 839.8 \text{ cm}^{-1}$ . Both collinear arrangements correspond to transition states (TSs) for  $r = 2.71$  bohrs,  $R = 7.60$  bohrs, and  $\theta = 0^\circ$  ( $D_e = 266.5 \text{ cm}^{-1}$ ), and  $r = 2.61$  bohrs,  $R = 5.80$  bohrs, and  $\theta = 180^\circ$  ( $D_e = 582.7 \text{ cm}^{-1}$ ). The  $\text{SN} \cdots \text{H}^- (^4A'')$  system exhibits a highly unusual PES with three minima (denoted as I, II, and III; cf. Fig. 1) and two transition states. The most stable

form (I) corresponds to a linear  $\text{H} \cdots \text{SN}^-$  configuration ( $r_e = 2.90$  bohrs,  $R_e = 5.60$  bohrs,  $\theta_e = 0^\circ$ ,  $D_e = 1247.5 \text{ cm}^{-1}$ ). The minimum of the intermediate stability (II) has a bent structure ( $r_e = 3.00$  bohrs,  $R_e = 4.35$  bohrs,  $\theta_e = 78.0^\circ$ ,  $D_e = 1161.68 \text{ cm}^{-1}$ ), and the third minimum again corresponds to a linear structure (III),  $\text{SN} \cdots \text{H}^-$  ( $r_e = 3.00$  bohrs,  $R_e = 5.25$  bohrs,  $\theta_e = 180^\circ$ ,  $D_e = 727.2 \text{ cm}^{-1}$ ). The linear and bent structures are separated by two transition states, one with  $r = 3.00$  bohrs,  $R = 6.20$  bohrs,  $\theta = 42.0^\circ$ , and  $D_e = 416.6 \text{ cm}^{-1}$  (between I and II) and the other characterized by  $r = 3.00$  bohrs,  $R = 7.35$  bohrs,  $\theta = 128.0^\circ$ , and  $D_e = 109.9 \text{ cm}^{-1}$  (between II and III). These potential barriers, connecting both bent and linear minima and exhibiting qualitatively drastically different rovibrational

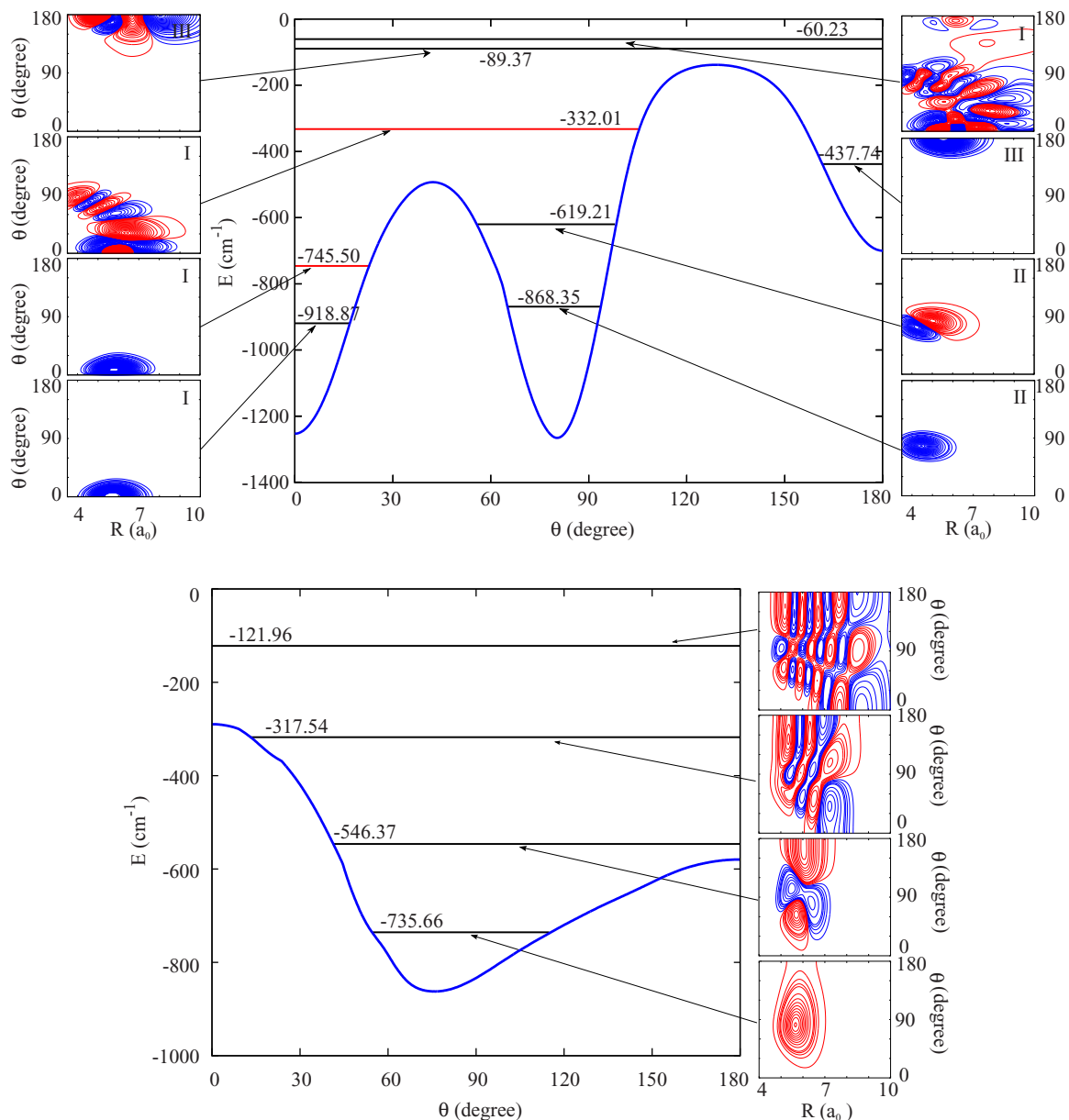


FIG. 3. Selected rovibrational wave functions from the SM [38] for  $\text{SN} \cdots \text{D}^-$  (top) and  $\text{SD} \cdots \text{N}^-$  (bottom) complexes and their localization in the corresponding potential (blue curve), where  $r$  is relaxed. The horizontal black lines indicate levels appearing when  $J \geq 0$ , whereas the red horizontal lines represent those appearing only when  $J \geq 1$ .  $R$  is in units of  $a_0$  and  $\theta$  is in units of degrees.  $E$  is the energy in units of  $\text{cm}^{-1}$ .

energy-level structures, are relatively low, making the  ${}^4A''$  electronic state of the  $[\text{S},\text{N},\text{H}]^-$  system a unique tool to investigate the characteristics of eigenstates located below and above the transition barriers.

Whereas the formation of a potential well for the  $\text{SH} \cdots \text{N}^-$  charge-induced complex is expected, the existence of three isomers for  $\text{SN} \cdots \text{H}^-$ , especially with bent and linear equilibrium structures and similar relative energies, is unique among molecular systems. As shown in Fig. 1, the favorable interactions between the outermost orbitals of the SH/SN and N/H monomers result from the lateral overlap between the  $\text{N}(2p)$  atomic orbital (AO) and the highest occupied molecular orbital (HOMO) of  $\text{SH}^-$ , which leads to one potential well. By contrast, the  $\text{H}(1s)$  AO may interact with the lone pair of S, the lone pair of N, or the  $\sigma$  lowest unoccupied molecular orbital

(LUMO) of  $\text{SN}^-$ , resulting in the three observed minima. Moreover, because all stationary points of both complexes are located below their respective lowest dissociation limits, the rovibrational levels lying above the transition barriers are bound and may exhibit large-amplitude motions extending over several minima. The complex potential shape observed has unique consequences for the spectroscopy of these weakly bound systems, as detailed below.

### B. Vibration-rotation energy-level structure

The full set of rovibrational levels for the  $\text{SH} \cdots \text{N}^-$ ,  $\text{SD} \cdots \text{N}^-$ ,  $\text{SN} \cdots \text{H}^-$ , and  $\text{SN} \cdots \text{D}^-$  complexes, up to dissociation, are reported in Tables S1–S4 and Figs. S1–S12 of the Supplemental Material (SM) [38] for total rotational angular momentum quantum numbers  $J = 0$  and 1. We also specify the

parity  $\varepsilon$  (+ or  $-$ ), which characterizes the symmetry of each rovibrational wave function with respect to space inversion. Along with  $J$ ,  $\varepsilon$  is a good quantum number regardless of the equilibrium structure of the molecule because the symmetry leading to  $J$  and  $\varepsilon$  relies on the properties of space rather than those of the molecular system [39–41].

For  $\text{SH}\cdots\text{N}^-$  and  $\text{SN}\cdots\text{H}^-$  (II), the pattern of the rovibrational energy levels within the corresponding potential wells is that of a bent asymmetric-top molecule. For the bound states located below the barrier,  $\text{SN}\cdots\text{H}^-$  (I) and  $\text{SN}\cdots\text{H}^-$  (III) are linear-type molecules. More intriguing is the energy-level structure above the barriers: the rovibrational energy levels assigned to the linear isomers I and III exhibit the well-known rovibrational pattern of a linear molecule (see Table I for a list of the energies and assignments of the lowest rovibrational levels for  $J = 0$  and 1 of  $\text{SN}\cdots\text{H}^-$ ). The bending levels with odd values of the bending mode ( $\nu_b$ ) are missing for  $J = 0$  and appear for  $J = 1$ , where they possess two parity components, as for linear molecules, instead of three (for  $J = 1$ ), as for asymmetric-top molecules. This behavior is confirmed for higher  $J$  values, where the linear-type levels form a pair with parity + and  $-$ , whereas the bent-type levels present  $(2J + 1)$  components. The simpler  $\text{SH}\cdots\text{N}^-$  case also conserves this rovibrational-level pattern. The  $(2J + 1)$  components of this asymmetric bent-type structure are also evidenced below and above the barriers, as is  $\text{SH}\cdots\text{N}^-$  (II). Regarding the states of the deuterated species, we observe qualitatively highly similar energy-level structures (see SM [38] for more details).

For  $\text{SN}\cdots\text{H}^-$  and  $\text{SH}\cdots\text{N}^-$  and their deuterated isotopologues, the rovibrational wave functions are mainly “concentrated” above the corresponding potential wells (see SM [38]). Some of the wave functions are depicted in Figs. 2 and 3. A clear nodal structure exists, regardless of whether the corresponding rovibrational state’s energy is below or above the barriers, making the assignment of the states straightforward. The wave functions thus show a “lock-in-mode” character over a large range of energies above the respective isomerization barriers. This indicates their localization, and we still observe a “bent-type” molecule for  $\text{SH}\cdots\text{N}^-$  and  $\text{SN}\cdots\text{H}^-$  (II) and a “linear-type” molecule for  $\text{SN}\cdots\text{H}^-$  (I) and  $\text{SN}\cdots\text{H}^-$  (III). Accordingly, the states conserve the memory of the equilibrium molecular type of the corresponding potential well above which they are located. We find that this vibrational memory effect is independent of the H/D exchange because we observe it for both H- and D-containing species.

#### IV. DISCUSSION

The nuclear-motion simulations provide insight into the energy-level structure above the potential barriers of compounds represented by multidimensional potentials. Many molecular systems have several isomeric forms. The spectra of these systems present unusual characteristics because of their complex nuclear motions. This is expected for microwave ( $\mu\text{w}$ ) and infrared (IR) spectra of the rovibrational transitions involving levels located below the potential barriers. However, for states located above the barriers, it is unclear how transitions corresponding to large-amplitude motions can be described. The present study presents a simple interpretation of

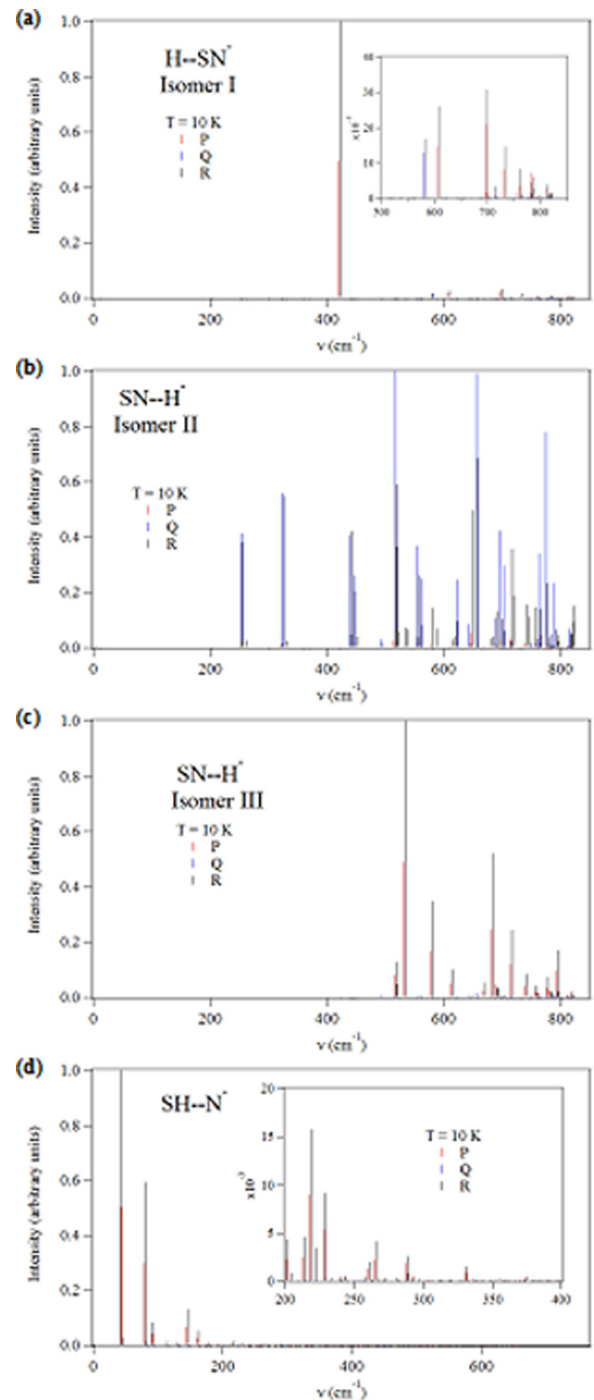


FIG. 4. Simulated  $\mu\text{w}$ -far IR spectra of  $\text{SN}\cdots\text{H}^-$  and  $\text{SH}\cdots\text{N}^-$ , with different isomers used as starting points: (a) linear  $\text{H}\cdots\text{SN}^-$  (Isomer I); (b) bent  $\text{SN}\cdots\text{H}^-$  (Isomer II); (c) linear  $\text{SN}\cdots\text{H}^-$  (Isomer III); (d)  $\text{SH}\cdots\text{N}^-$ . The inset in (d) shows the transitions populating the levels above the potential barrier. The spectra are normalized to the most intense band. They are issued from the corresponding lowest  $J = 1$ ,  $\varepsilon = -$  level. The zero energy is taken as the position of the  $J = 1$ ,  $\varepsilon = -$  level of  $\text{SN}\cdots\text{H}^-$  (Isomer II) in (a–c) and the  $J = 1$ ,  $\varepsilon = -$  level of  $\text{SH}\cdots\text{N}^-$  in (d). Most transitions populate levels located above the potential barriers.  $\nu$  is the frequency in units of  $\text{cm}^{-1}$ .

the spectra since the analysis relies only on the structure of the isomer used as a starting point. For illustration, Fig. 4 shows

the simulated  $\mu\text{w}$ -IR spectra of  $\text{SN}\cdots\text{H}^-$  and  $\text{SH}\cdots\text{N}^-$ , with different isomers used to generate the spectra. For instance, we display the low-frequency part of the simulated  $\mu\text{w}$ -far IR spectra of  $\text{SN}\cdots\text{H}^-$  and of  $\text{SH}\cdots\text{N}^-$  where the linear  $\text{H}\cdots\text{SN}^-$  (Isomer I), the bent  $\text{SN}\cdots\text{H}^-$  (Isomer II), the linear  $\text{SN}\cdots\text{H}^-$  (Isomer III), and the bent  $\text{SH}\cdots\text{N}^-$  isomers are used as a starting point, i.e., we considered transitions from their ground vibrationless level. For these simulations, we used a temperature  $T = 10$  K. These spectra are structured with distinct P, Q, and R branches. The transitions populating the levels located above the potential barriers have appreciable nonzero intensities.

Vibrational-rotational spectroscopy is routinely used in chemistry, physics, astrophysics, materials sciences, and biochemistry to understand the structure and dynamics of molecular systems and probe reaction processes. Baraban *et al.* [4] recently illustrated how vibrational modes can be distinguished between those actively involved in isomerization and those that are passive bystanders above an isomerization barrier and revealed that it is possible to obtain high-resolution vibrational information on the isomerizing levels all the way to the barrier and beyond. However, Baraban *et al.* also noted that a limitation of their analysis is the lack of treatment by a multidimensional analysis. Our findings suggest that the expansion to multidimensions in the potential does not destroy such structure-potential correspondence. Moreover, our work demonstrates the existence of a vibrational memory effect. This is made possible by the qualitatively drastically different energy-level sets supported by bent and linear molecular systems. This study provides the extension of such behavior in molecular physics, where the potential wells are disordered in two or three dimensions.

## V. CONCLUSIONS

Through the analysis of the eigenenergies and wave functions of the rovibrational states of a polyatomic molecular system located below and above the potential barriers, we show that these wave functions are well localized and that they preserve the memory of the isomeric forms they originate from. We also demonstrate the existence of a strong vibrational memory effect above isomerization barriers. These findings may help our understanding of the quantum localizations, in one dimension, observed for some molecular systems, for short-range interacting bosons, for electrons in GaAs potential wells, and in solid-state quantum dots. This work extends these findings to multidimensional potentials.

## ACKNOWLEDGMENTS

This study was undertaken while M.H. was a Visiting Professor at King Saud University. The support of the Visiting Professor Program at King Saud University is hereby gratefully acknowledged. J.S.F. and A.G.C. thank the Université Paris-Est for the Professeur Invité stays. We acknowledge the financial support from a Marie Curie International Research Staff Exchange Scheme Fellowship within the 7th European Community Framework Program under Grant No. PIRSES-GA-2012-317544 and the COST Action CM1405 MOLIM. A.G.C. was supported by the Scientific Research Fund of Hungary (OTKA, Grant No. NK83583). Computer time for this study was provided by the Mésocentre de Calcul Intensif Aquitaine computing facilities of Université de Bordeaux and Université de Pau et des Pays de l'Adour.

- 
- [1] G. Herzberg, in *Molecular Spectra and Molecular Structure II. Infrared and Raman Spectra of Polyatomic Molecules* (Van Nostrand, Princeton, NJ, 1945).
- [2] G. Ch. Mellau, *J. Chem. Phys.* **134**, 194302 (2011).
- [3] M. Herman and D. S. Perry, *Phys. Chem. Chem. Phys.* **15**, 9970 (2013).
- [4] J. H. Baraban, P. B. Changala, G. Ch. Mellau, J. F. Stanton, A. J. Merer, and R. W. Field, *Science* **350**, 1338 (2015).
- [5] Z. Bačić and J. C. Light, *J. Chem. Phys.* **86**, 3065 (1987).
- [6] P. R. Schreiner, H. P. Reisenauer, F. C. Pickard, A. C. Simmonett, W. D. Allen, E. Mátyus, and A. G. Császár, *Nature* **453**, 906 (2008).
- [7] S. Zou, J. M. Bowman, and A. Brown, *J. Chem. Phys.* **118**, 10012 (2003).
- [8] R. Otto, J. Ma, A. W. Ray, J. S. Daluz, J. Li, H. Guo, and R. E. Continetti, *Science* **343**, 396 (2014).
- [9] A. von Zastrow, J. Onvlee, S. N. Vogels, G. C. Groenenboom, A. van der Avoird, and S. Y. T. van de Meerakker, *Nat. Chem.* **6**, 216 (2014).
- [10] H. Kohguchi, T. Suzuki, and M. H. Alexander, *Science* **294**, 832 (2001).
- [11] B. Yang, P. Zhang, X. Wang, P. C. Stancil, J. M. Bowman, N. Balakrishnan, and R. C. Forrey, *Nat. Commun.* **6**, 6629 (2015).
- [12] M. Tizniti, S. D. Le Picard, F. Lique, C. Berteloite, A. Canosa, M. H. Alexander, and I. R. Sims, *Nat. Chem.* **6**, 141 (2014).
- [13] I. L. Aleiner, B. L. Altshuler, and G. V. Shlyapnikov, *Nat. Phys.* **6**, 900 (2010).
- [14] M. Heiblum, M. V. Fischetti, W. P. Dumke, D. J. Frank, I. M. Anderson, C. M. Knodler, and L. Osterling, *Phys. Rev. Lett.* **58**, 816 (1987).
- [15] Y. C. Chen, C.-C. Lee, and F. Flory, *J. Nanophotonics* **8**, 083090 (2014).
- [16] M. Belloni and R. W. Robinett, *Phys. Rep.* **540**, 25 (2014).
- [17] T. Trabelsi, Y. Ajili, S. Ben Yaghlane, N.-E. Jaidane, M. Mogren Al-Mogren, J. S. Francisco, and M. Hochlaf, *J. Chem. Phys.* **143**, 034303 (2015).
- [18] P. Halvick, T. Stoecklin, F. Lique, and M. Hochlaf, *J. Chem. Phys.* **135**, 044312 (2011).
- [19] F. Lique, J. Klos, and M. Hochlaf, *Phys. Chem. Chem. Phys.* **12**, 15672 (2010).
- [20] Y. N. Kalugina, I. A. Buryak, Y. Ajili, A. A. Vigasin, N. E. Jaidane, and M. Hochlaf, *J. Chem. Phys.* **140**, 234310 (2014).
- [21] Y. Ajili, K. Hammami, N. E. Jaidane, M. Lanza, Y. N. Kalugina, F. Lique, and M. Hochlaf, *Phys. Chem. Chem. Phys.* **15**, 10062 (2013).

- [22] Y. Tebai, N.-E. Jaidane, D. Ben Abdallah, Ph. Halvick, T. Stoecklin, and M. Hochlaf, *J. Chem. Phys.* **141**, 174305 (2014).
- [23] M. Mogren Al Mogren, O. Denis-Alpizar, D. Ben Abdallah, T. Stoecklin, P. Halvick, M.-L. Senent, and M. Hochlaf, *J. Chem. Phys.* **141**, 044308 (2014).
- [24] G. Knizia, T. B. Adler, and H.-J. Werner, *J. Chem. Phys.* **130**, 054104 (2009).
- [25] G. Rauhut, G. Knizia, and H.-J. Werner, *J. Chem. Phys.* **130**, 054105 (2009).
- [26] MOLPRO is a package of *ab initio* programs written by H.-J. Werner, P. J. Knowles, G. Knizia, F. R. Manby, M. Schütz, P. Celani, W. Györffy, D. Kats, T. Korona, R. Lindh, A. Mitrushenkov, G. Rauhut, K. R. Shamasundar, T. B. Adler, R. D. Amos, A. Bernhardsson, A. Berning, D. L. Cooper, M. J. O. Deegan, A. J. Dobbyn, F. Eckert, E. Goll, C. Hampel, A. Hesselmann, G. Hetzer, T. Hrenar, G. Jansen, C. Köppl, Y. Liu, A. W. Lloyd, R. A. Mata, A. J. May, S. J. McNicholas, W. Meyer, M. E. Mura, A. Nicklaß, D. P. O'Neill, P. Palmieri, D. Peng, K. Pflüger, R. Pitzer, M. Reiher, T. Shiozaki, H. Stoll, A. J. Stone, R. Tarroni, T. Thorsteinsson, and M. Wang, see <http://www.molpro.net>.
- [27] T. H. Dunning, *J. Chem. Phys.* **90**, 1007 (1989).
- [28] R. A. Kendall, T. H. Dunning, and R. J. Harrison, *J. Chem. Phys.* **96**, 6796 (1992).
- [29] W. Klopper, *Mol. Phys.* **99**, 481 (2001).
- [30] F. Weigend, A. Köhn, and C. Hättig, *J. Chem. Phys.* **116**, 3175 (2002).
- [31] S. F. Boys and F. Bernardi, *Mol. Phys.* **19**, 553 (1970).
- [32] T. S. Ho and H. Rabitz, *J. Chem. Phys.* **104**, 2584 (1996).
- [33] T. Stoecklin and A. Voronin, *Phys. Rev. A* **72**, 042714 (2005).
- [34] J. M. Hutson, BOUND computer code, version 5, distributed by Collaborative Computational Project No. 6 of the Science and Engineering Research Council, UK, 1993.
- [35] K. P. Huber and G. Herzberg, in *Molecular Spectra and Molecular Structure. IV. Constants of Diatomic Molecules* (Van Nostrand Reinhold, New York, 1979).
- [36] R. M. Whitnell and J. C. Light, *J. Chem. Phys.* **90**, 1774 (1989).
- [37] T. Stoecklin, F. Lique, and M. Hochlaf, *Phys. Chem. Chem. Phys.* **15**, 13818 (2013).
- [38] See Supplemental Material at <http://link.aps.org/supplemental/10.1103/PhysRevA.93.052514> for the calculated ro-vibrational energies and wave functions of  $\text{SH}\cdots\text{N}^-(^4A'')$ , of  $\text{SD}\cdots\text{N}^-(^4A'')$ , of  $\text{SN}\cdots\text{H}^-(^4A'')$  and of  $\text{SN}\cdots\text{H}^-(^4A'')$  from the corresponding 3D-PESs for  $J = 0$  and 1.
- [39] T. Oka, *J. Mol. Spectrosc.* **48**, 503 (1973).
- [40] J. M. Hollas, *Modern Spectroscopy*, 4th ed. (Wiley, Chichester, UK, 2004).
- [41] L. D. Landau and E. M. Lifshitz, *Quantum Mechanics, Nonrelativistic Theory* (Fizmatgiz, Moscow, 1963).